Measurement of Peeling Mode Edge Current Profile Dynamics

M. W. Bongard, R. J. Fonck, C. C. Hegna, A. J. Redd, and D. J. Schlossberg

Phys. Rev. Lett. **107**, 035003 — Published 12 July 2011

DOI: 10.1103/PhysRevLett.107.035003

Measurement of Peeling Mode Edge Current Profile Dynamics

M.W. Bongard, R.J. Fonck, C.C. Hegna, A.J. Redd, and D.J. Schlossberg
Department of Engineering Physics, University of Wisconsin-Madison,
1500 Engineering Drive, Madison, Wisconsin 53706, USA

Peeling modes, an instability mechanism underlying deleterious Edge Localized Mode (ELM) activity in fusion-grade plasmas, are observed at the edge of limited plasmas in a low aspect ratio tokamak under conditions of high edge current density ($J_{edge} \sim 0.1$ MA/m^2) and low magnetic field ($B \sim 0.1$ T). They generate edge localized, electromagnetic activity with low toroidal mode numbers $n \leq 3$ and amplitudes that scale strongly with measured J_{edge}/B instability drive, consistent with theory. ELM-like field-aligned, current-carrying filaments form from an initial current-hole J_{edge} perturbation that detach and propagate outward.

PACS numbers: 52.55.Fa, 52.35.Py, 52.70.Ds

The performance of next-step magnetic fusion devices such as ITER [1] depends critically on the magnetohydrodynamic (MHD) stability of the plasma boundary. Steep pressure gradients and large currents exist in the edge of plasmas in the enhanced confinement (H-mode) regime [2] where such devices must operate to achieve their mission. These extreme conditions drive periodic instabilities that transiently degrade edge confinement, releasing particles and large fractions of the stored plasma energy on rapid (100 μs) timescales [3]. Known as Edge Localized Modes (ELMs) [4], these instabilities generate field-aligned filamentary structures that propagate from the plasma edge to material surfaces [5]. ELMs affect total fusion gain by limiting the plasma pressure, and may damage vessel components due to high local heat fluxes. Accurate prediction of edge instability thresholds and an understanding of their resultant dynamical processes are needed to avoid or mitigate these deleterious effects.

An instability model that invokes the interaction between two classes of edge-localized, ideal MHD instabilities - pressure-driven ballooning modes with high toroidal mode number n, and current-driven peeling modes with low n - provides a framework to describe ELM onset. This peeling-ballooning model [6] places limits on the edge pressure gradient ∇p and parallel current density $J_\parallel$. Violating them is known to trigger an ELM, thereby relaxing the instability drive. Experimental stability boundaries at highest performance are well-described by the onset of peeling-ballooning modes at intermediate $n \sim 3-30$ [7]. Nonlinear simulations that evolve unstable peeling-ballooning mode structures exhibit filament generation similar to that seen in experiment [8]. These models are being extended to experimentally relevant magnetic topologies and plasma parameters to predict nonlinear edge dynamics and their resultant machine power deposition with confidence [9, 10].

Detailed edge measurements are required to validate the sensitivity of stability boundaries to the equilibrium pressure profile, current profile, and cross-section shape, as well as the detailed dynamics of the instability. However, measurements of the radial edge current density profile $J_{edge}(R)$ have not been readily available with sufficient spatial and temporal accuracy for such validation. Localized measurements from Li beam polarimetry in DIII-D [11] have lent support to pressure-driven current models typically invoked in peeling-ballooning analyses, but have not yet resolved the critical dynamical evolution of $J_{edge}(R,t)$ during an ELM event [12].

This Letter reports first measurements of $J_{edge}(R,t)$ at sufficiently high time resolution to resolve the ELM-like filament evolution arising from peeling modes in the Pegasus Toroidal Experiment [13]. It shows that peeling mode amplitudes rise rapidly with their predicted drive, and that an ejected current filament evolves concurrently with formation of a local current-hole perturbation in $J_{edge}(R)$. The initial acceleration of the filament from the plasma edge and subsequent propagation at constant radial velocity is qualitatively consistent with a model invoking just such a transient formation of a current hole in the plasma edge region [14].

Peeling modes are edge-localized, ideal external kink instabilities. They are driven by edge current and stabilized by the pressure gradient ∇p and magnetic shear s, which is embodied in the analytic stability criterion for peeling modes [15] at finite aspect ratio A:

$$\sqrt{1-4D_M} > 1 + \frac{1}{\pi q'} \oint \frac{\mu_o J_\parallel B}{R^2 B_p^3}\, dl. \tag{1}$$

Here, $D_M \propto \nabla p$ is the Mercier index [16], $J_\parallel$ the edge current density along the magnetic field $\mathbf{B}$, q' the derivative of the safety factor q with respect to the poloidal flux ($\propto s$), B_p the poloidal field at major radius R, and the contour is taken on an edge flux surface. In the limit of low pressure, high-A, and weak shaping, the peeling instability drive is proportional to $J_\parallel/B$ at fixed ∇p.

With its low toroidal field B_ϕ for a given plasma current I_p, the spherical tokamak (ST) naturally leads to high values of this $J_\parallel/B$ instability drive, and offers unique opportunities for detailed study of peeling mode dynamics. Pegasus is an ultralow-A ST with variable geometry, $I_p < 200$ kA, $B_\phi < 0.16$ T, minor radius 0.20 m $< a \leq 0.39$ m, and major radius $R_0 \leq 0.45$ m. In contrast to the pressure-driven current occurring in the H-mode edge of large tokamaks, J_{edge} is provided here by large skin currents during strong plasma current ramps ($\dot{I}_p \leq 50$ MA/s) even though plasmas have a limited magnetic topology and standard (L-mode) confinement. $J_\parallel/B$ is ~ 1 MA/(m^2-T) at nominal B_ϕ, sufficient to exceed the peeling instability boundary of Eq. (1).

The $J_\parallel/B$ peeling drive is strongest during the initial I_p rampup of Ohmic discharges. During this time, edge localized, field-aligned filament perturbations are evident on fast visible images of the plasma at exposure times $\lesssim 30$ μs, reflecting a relatively short coherence time. A representative image of a small plasma ($R_0 \approx 0.26$ m, $a \approx 0.20$ m) obtained during a 10 μs interval shows these filaments predominantly on the outer, low-field side in Fig. 1. Contrast in the fast perturbations has been enhanced by subtracting the average emission of the previous 270 μs period. High poloidal coherence is evident, with the intensity of the filament structures simultaneously rising and falling in time. They appear to rotate with the bulk plasma, detach from the edge after $\sim 30-50$ μs, and propagate radially outward.

Magnetic pickup (Mirnov) coils near the plasma edge indicate these large perturbed structures are electromagnetic, rather than electrostatic, in nature. These magnetic fluctuation signals are uncorrelated with electrostatic probe fluctuation measurements at the same toroidal location.

Mode spatial structure is measured with a Mirnov probe array that is placed tangent to the plasma edge at arbitrary R at height $Z = 0$ from the device midplane. It consists of a linear array of six coils equally spaced tangentially to measure B_Z along 0.21 m in the toroidal direction (equivalent to a toroidal angular span $\Delta\phi \sim 15^\circ$ when $R \sim R_{edge}$), plus a seventh coil radially separated from the array by ~ 9 cm. This allows a determination of n by toroidal cross-phase analysis, and provides an estimate of the poloidal mode number m in the lab frame by measuring the radial decay of the mode amplitude, $\propto R^{-m}$ in vacuum. A second estimate of m is made by employing a separate, vertically displaced Mirnov coil at comparable radial location and toroidal angle and performing poloidal cross-phase analysis in the lab frame.

A determination of m in the plasma frame requires the use of an angular mapping derived from equilibrium analysis that can account for the varying field line pitch set by the safety factor; *i.e.* $m = f(q)m_{lab}$ [17]. For plasmas similar to those in Fig. 1, $f(q) \sim 3 - 7$ when mapped to the measurement locations.

The observed edge instability properties are consistent with those of peeling modes. Spectral and spatial analysis of coherent MHD fluctuations during the I_p ramp indicate $10 \lesssim m_{lab}/n \lesssim 30$ with low $n \leq 3$ and high $m_{lab} \gtrsim 10$. Magnetic equilibrium reconstructions using standard external magnetics measurements [18] locate resonant flux surfaces where $q_{res} = m_{lab}/n$ at a normalized poloidal flux $\psi_N > 0.9$. This implies the true resonance is highly localized at or just exterior to the plasma edge, consistent with the expected external kink structure of peeling modes.

A novel internal magnetic probe employing Hall effect sensors [19] is used to measure the detailed spatial and temporal properties of $J_{edge}(R,t)$ during the edge instability. It provides a local measurement of $B_Z(R,t)$ at a height $Z = .125$ m, with negligible plasma perturbation and high temporal resolution. With estimates of the plasma geometry from magnetic equilibrium reconstructions, these field measurements are used to infer the local toroidal current density $J_\phi(R,t)$ from Ampère's Law [20]:

$$\mu_0 J_\phi = -\frac{B_Z}{\kappa^2 (R - R_0)} \left(1 - \frac{Z^2 R_0}{\kappa^2 R (R - R_0)^2}\right) - \frac{dB_Z}{dR} \left(1 + \frac{Z^2}{\kappa^4 (R - R_0)^2}\right). \quad (2)$$

SI units are used here, R and Z are the sensor locations, and shaping is estimated to first order by an elliptical cross-section of ellipticity κ centered at R_0. Spline fitting of $B_Z(R)$ is used to extract dB_Z/dR. The effects of higher-order shaping, such as plasma triangularity δ and Shafranov shift [21], are negligible within the experimental errors in $J_\phi(R)$.

Figure 2 shows profiles of the measured $B_Z(R)$ [2(a)] and inferred $J_\phi(R)$ [2(b)] from two repeated discharges during an MHD quiescent phase. A current density of 96 ± 9 kA/m^2 is found with $I_p = 115$ kA for $0.50 < R < 0.55$ m with $R_0 \approx 0.36$ m and $a \approx 0.30$ m. It decays to zero at $R = 0.65$ m, in agreement with estimates of R_{edge} at $Z = .125$ m from the visible imaging.

Edge instability characteristics were measured in scans that varied the $J_\parallel/B$ peeling drive by using $\dot{I}_p$ to control $J_\parallel$ at varied B. Discharges had a constant $\dot{I}_p$ of $\{30, 15, 10\}$ MA/s with $B_\phi = \{0.08, 0.11, 0.13, 0.16\}$ T. Shape evolution was matched during the I_p ramp to minimize its geometric influence, ending with nominal values of $R_0 = 0.36$ m, $a = 0.29$ m, $\kappa = 1.5$, and $\delta = 0.44$. An average density $\bar{n}_e \approx 1 \times 10^{19}$ m^{-3} was maintained in all cases, resulting in a low Greenwald fraction $n/n_G = \{0.13, 0.17, 0.21\}$ for the respective levels of $\dot{I}_p$. The low density, modest B_ϕ and relatively low edge temperatures ($T_e < 0.2$ keV) of these L-mode discharges place them in the low-pressure peeling regime, with negligible ∇p ballooning stabilization.

As expected for peeling modes, their observed amplitude is strongly dependent on the magnitude of the $J_\parallel/B$ drive. This is inferred from experiment by the quantity J_ϕ/B_ϕ, as J_ϕ closely approximates $J_\parallel$ in L-mode due to the lack of strong ∇p-driven currents and $B_\phi/B \sim 1$. For fixed J_ϕ, mode onset was delayed and its amplitude reduced with increasing B_ϕ; similarly, for fixed field, activity increased with J_ϕ. At lowest J_ϕ/B_ϕ, peeling activity was mitigated throughout the I_p ramp. Figure 3(a) shows the low-n mode amplitude increasing approximately two orders of magnitude with a factor-of-5 variation in the measured J_ϕ/B_ϕ. J_ϕ has been parameterized in the figure by its value near the top of the $J_\phi(R)$ profile where $d^2 J_\phi/dR^2$ is an extremum, *e.g.* $R = 0.54$ m in Fig. 2.

The analytic peeling instability condition is exceeded for reconstructed equilibria obtained during periods of mode activity. A representative calculation [Fig. 3(b)] shows the ratio of the right and and left hand sides of Eq. (1) plotted from a reconstruction with $J_\parallel(\psi)$ constrained by internal Hall measurements. Instability is indicated when this ratio exceeds unity, in this case by more than a factor of two. Ideal stability analysis of the equilibrium with DCON [22] finds the plasma unstable to an $n = 1$ external kink, consistent with the existence of $n = 1$ peeling modes.

Figure 4 shows the complex temporal evolution of $J_{edge}(R,t)$ over 45 μs as a filament is generated and ejected from the plasma edge. This data is taken from the same discharge sets as Fig. 2, when $I_p = 96$ kA.

The edge current channel is initially displaced outward, with J_{edge} increasing at outermost radii while inwardly decreasing to form a "current-hole" inside of the peak J_{edge} region. The magnitude of the perturbation grows, narrows in width, and propagates radially outward. The innermost current distribution begins to recover after 30 μs, and approaches pre-crash values by 45 μs.

The net toroidal current carried by the filament I_f is estimated by assuming a circular cross-section with radius δ_b and diameter equal to the measured FWHM of the J_ϕ centroid. For $t = 45$ μs in Fig. 4, this leads to $I_f \sim 115$ A. This is only an estimate, since $J_\phi(R,t)$ given by Eq. (2) is derived assuming toroidal symmetry, while the filament is a helical perturbation on this equilibrium. A second estimate of I_f is obtained by equating the filament's self-field to the local B_Z perturbation assuming a characteristic flattening length of δ_b, implying $\mu_0 I_f \approx 2\pi\delta_b^2 dB_Z/dR$. Taking δ_b to be the filament width, this gives a comparable estimate of $I_f \sim 220$ A. Such currents are $\lesssim 0.2\%$ of I_p. More precise estimates of I_f will require 3-D perturbation modeling.

The current-hole perturbation in $J_{edge}(R)$ that becomes a radially propagating current filament is a fundamental feature of models describing ELM dynamics [14]. The magnetostatic repulsion of the filament with its accompanying transient hole generates an additional electromagnetic contribution to the radial forces arising from intrinsic curvature and ∇B drifts in a tokamak [23]. Such forces induce charge separation in the filament, causing radial propagation at a constant characteristic $E \times B$ velocity $v_{E\times B}$, which is dependent on various theoretical closures for the parallel current flow [24].

The added magnetostatic repulsion can also generate transient radial acceleration, and contribute to filament dynamics when its acceleration drive $\dot{v}$ dominates that from curvature $\dot{v}_\kappa$ [14]. This is significant when $\dot{v}/\dot{v}_\kappa = 2R_0/\beta_b d \geq 1$, where d is the filament-hole separation and $\beta_b = 2\mu_0 n_e T_e/B_b \approx 8\pi^2\delta_b^2 n_e T_e/\mu_0 I_f^2$ is a normalized pressure in a circular cross-section filament to its self-field B_b at one radius δ_b. This condition is satisfied, with $1.8 \lesssim \dot{v}/\dot{v}_\kappa \lesssim 6.5$, when taking representative experimental parameters for the case in Fig. 4: $n_e = 1\times10^{18}$ m^{-3}, $T_e = 10$ eV, $I_f = 115 - 220$ A, $R_0 = 0.36$ m, $\delta_b = 0.03$ m, and an initial separation $d = 2\delta_b$. Furthermore, for $B_\phi(R_0) \approx 0.16$ T, a filament connection length $L_\parallel \approx 20$ m from equilibrium field line following in Pegasus geometry, and Spitzer resistivity, the later constant-velocity phase of the filament trajectory is best described for these conditions by the ideal ballooning closure of Myra and D'Ippolito [24], which gives to order-unity corrections $v_{E\times B} = c_s\delta_b^{1/2}/R^{1/2} \approx 8$ km/s, where c_s is the ion sound speed.

Filaments appear to accelerate radially outward simultaneously with the development of the current-hole perturbation. High-speed imaging was available to track the radial location of ejected filaments during peeling instability in discharges comparable to those in Fig. 4 but with a somewhat faster filament evolution. A typical trajectory is plotted in Fig. 5, which indicates an early radial acceleration phase with $a_R \approx 1 - 3\times10^7$ m/s^2 followed by a phase with near-constant radial velocity $v_R = 4.1 \pm 0.2$ km/s after ≈ 35 μs. This v_R is comparable to the estimates of $v_{E\times B}$ from the ideal ballooning scaling mentioned above. Detailed 3-D resistive MHD models of filament generation and propagation are needed to describe the entire filament trajectory.

These measurements show that peeling modes generate current-carrying filaments from the edge. They detach and radially accelerate during the formation and decay of an inboard current-hole, and then propagate at a constant v_R. The mode amplitudes depend strongly on the measured $J_\parallel/B$ drive. These observations qualitatively support existing models of the peeling instability underlying ELM filament formation.

The authors thank B. Lewicki, B. Kujak-Ford, and G. Winz for their assistance. This work is supported by U.S. DOE Grants DE-FG02-96ER54375 and DE-FG02-86ER53218.

[1] M. Shimada *et al.*, Nucl. Fusion **47**, S1 (2007).
[2] F. Wagner *et al.*, Phys. Rev. Lett. **49**, 1408 (1982).
[3] A. Loarte *et al.*, Plasma Phys. Control. Fusion **44**, 1815 (2002).
[4] J. W. Connor, Plasma Phys. Control. Fusion **40**, 531 (1998).
[5] A. Kirk *et al.*, Phys. Rev. Lett. **96**, 185001 (2006).
[6] P. B. Snyder *et al.*, Phys. Plasmas **9**, 2037 (2002).
[7] P. Snyder *et al.*, Nucl. Fusion **49**, 085035 (2009).
[8] P. B. Snyder, H. R. Wilson, and X. Q. Xu, Phys. Plasmas **12**, 056115 (2005).
[9] G. T. A. Huysmans *et al.*, Plasma Phys. Control. Fusion **51**, 124012 (2009).
[10] B. Burke, Ph.D. thesis, Univ. Wisconsin-Madison (2010).
[11] D. M. Thomas *et al.*, Phys. Plasmas **12**, 056123 (2005).
[12] C. Maggi, Nucl. Fusion **50**, 066001 (2010).
[13] G. Garstka *et al.*, Nucl. Fusion **46**, S603 (2006).
[14] J. R. Myra, Phys. Plasmas **14**, 102314 (2007).
[15] J. W. Connor *et al.*, Phys. Plasmas **5**, 2687 (1998).
[16] C. Mercier, Nucl. Fusion **1**, 47 (1960).
[17] W. D'haeseleer *et al.*, *Flux Coordinates and Magnetic Field Structure* (Springer-Verlag, 1991).
[18] A. Sontag *et al.*, Nucl. Fusion **48**, 095006 (2008).
[19] M. Bongard *et al.*, Rev. Sci. Instrum. **81**, 10E105 (2010).
[20] C. Petty *et al.*, Nucl. Fusion **42**, 1124 (2002).
[21] C. C. Petty, P. A. Politzer, and Y. R. Lin-Liu, Plasma Phys. Control. Fusion **47**, 1077 (2005).
[22] A. H. Glasser and M. S. Chance, Bull. Am. Phys. Soc. **42**, 1848 (1997).
[23] S. I. Krasheninnikov, D. A. D'Ippolito, and J. R. Myra, J. Plasma Physics **74**, 679 (2008).
[24] J. R. Myra and D. A. D'Ippolito, Phys. Plasmas **12**, 092511 (2005).

FIGURES

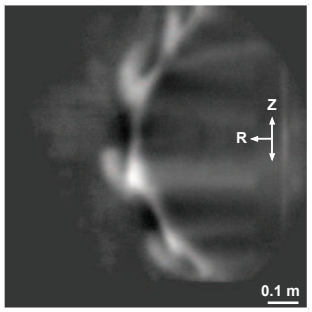

Figure 1. Contrast-enhanced visible light image of peeling activity in 10 μs interval.

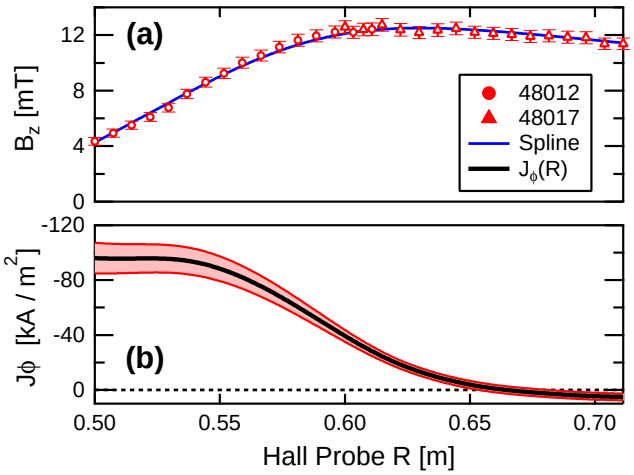

Figure 2. (Color online.) (a) Internal $B_Z(R)$ from repeated discharges, fit with smoothing spline. (b) Inferred $J_\phi(R)$.

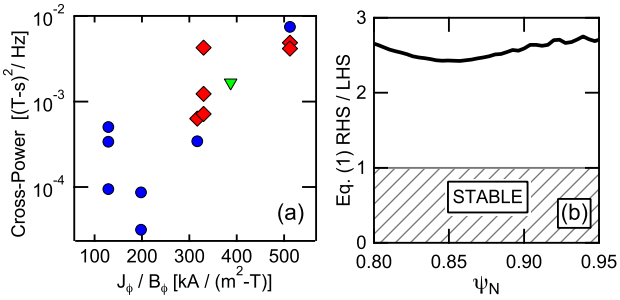

Figure 3. (Color online.) (a) MHD fluctuation power and toroidal mode number from peeling drive scan. Circles, $n = 1$; diamonds, $n = 2$; triangle, $n = 3$. (b) Analytic peeling stability criterion from experimental equilibrium.

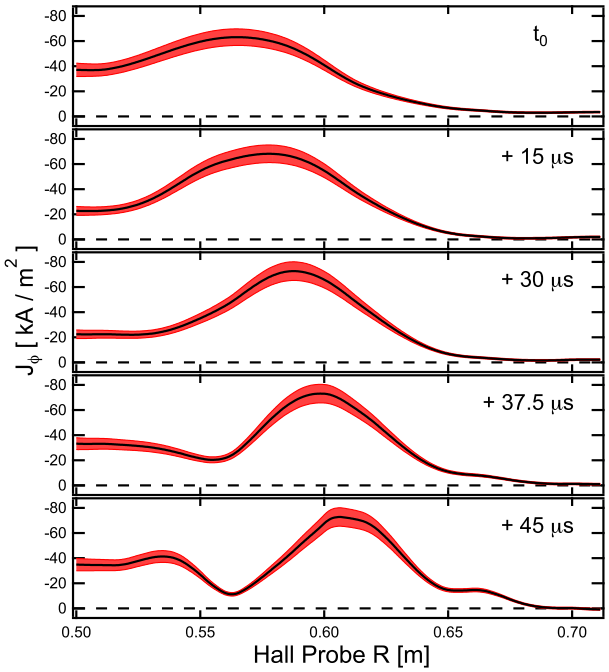

Figure 4. (Color online.) $J_\phi(R, t)$ during filament creation.

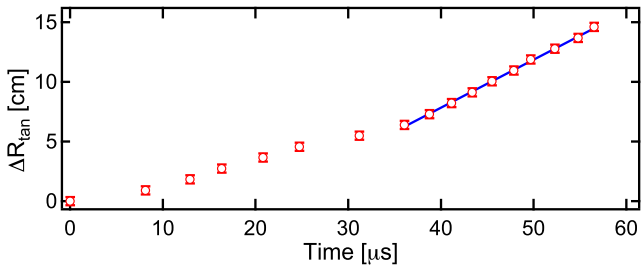

Figure 5. (Color online.) Filament radial displacement versus time. For $t \gtrsim 35$ μs, $v_R \approx 4$ km/s (solid).